Delft University of Technology

Adaptive Incremental Nonlinear Dynamic Inversion Flight Control for Consistent Handling Qualities

Smit, B.; Pollack, T.S.C.; van Kampen, E.

Adaptive Incremental Nonlinear Dynamic Inversion Flight Control for Consistent Handling Qualities

B. Smit [*], T.S.C. Pollack[†], and E. van Kampen[‡]
Delft University of Technology, 2629HS Delft, The Netherlands

Control augmentation systems based on Incremental Nonlinear Dynamic Inversion (INDI) are able to provide high-performance nonlinear control without a holistic model. Considering an angular rate control law for a fixed-wing aircraft, only a control effectiveness (CE) model and angular acceleration measurement feedback is required. Despite enhanced robustness against parametric model mismatches due to reduced model dependency, the performance of INDI-based control laws can still vary due to inaccurate CE models. This paper confirms that longitudinal centre of gravity (CG) shifts and CE uncertainty result in varying handling qualities and stability (HQ&S) characteristics. An adaptive solution using Least-Mean-Square (LMS) based parameter estimation is investigated to address these variations. The results demonstrate that online CE model correction result in reduced HQ&S variation. However, it was found that some flight conditions together with adverse CG shifts could lead to violation of the time-scale separation assumption that underlies the adaptive control law design. As this assumption is inherent to the INDI control design itself as well, online CE model correction is only partly able to resolve the resulting performance variations.

Nomenclature

C	kg	Fuel tank capacity
C	-	Correction factor
$\bar{c}$	m	Mean Aerodynamic Chord
$C_{m_{\delta_e}}$	-	Elevator aerodynamic pitch control coefficient
e	deg/s	Pitch rate tracking error
e_G	s^{-2}	Control effectiveness estimation error
G	s^{-2}	Control effectiveness
H	-	Transfer function
I	$kg \cdot m^2$	Mass moment of inertia
K	-	Control law design parameter
M	kg	Mass
$\mathcal{M}$	Nm	Pitching moment
n_s	-	Number of observation window samples
N	-	Size of data vector
p	$deg \cdot s^{-1}$	Roll rate
q	$deg \cdot s^{-1}$	Pitch rate
$\bar{q}$	Pa	Dynamic pressure
r	$deg \cdot s^{-1}$	Yaw rate
s	-	Laplace operator
s	s^{-4}	Cumulative Moving Standard Deviation Window variance
S	m^2	Reference surface area
t	s	Time
T_s	s	Sampling time
$\boldsymbol{u}$	deg	Control input vector
$\boldsymbol{x}$	-	State vector

[*]Graduate Student, Control and Simulation Division, Faculty of Aerospace Engineering, Kluyverweg 1, 2629HS Delft, the Netherlands
[†]Ph.D. Student, Control and Simulation Division, Faculty of Aerospace Engineering, Kluyverweg 1, 2629HS Delft, the Netherlands
[‡]Assistant Professor, Control and Simulation Division, Faculty of Aerospace Engineering, Kluyverweg 1, 2629HS Delft, the Netherlands

α	deg	Angle-of-attack
δ_e	*deg*	Elevator deflection
Δ	-	Incremental notation
ν_q	$deg \cdot s^{-2}$	Virtual pitch control input
μ	-	LMS adaption gain
ϕ	$deg \cdot s^{-2}$	Regression basis function
ζ	-	Damping coefficient
ω	rad/s	Natural frequency
$\|\cdot\|_\infty$	-	Infinity norm.

I. Introduction

The ongoing pursuit of increasing flight capabilities of high-performance aircraft is driving control system design based on classical control theory to its boundaries. High angle-of-attack flight, increased airspeeds, and enhanced agility are desired improvements to enlarge the operational limits and therefore increase the platform capability [1–3]. At such flight conditions, airframe dynamics are significantly nonlinear due to inertial coupling and strongly nonlinear aerodynamic effects. The consequence is that the segmented linear model assumption used for classical control law design becomes increasingly difficult to maintain [1, 4, 5]. This problem causes degraded tracking performance which can lead to increased pilot workload or even an abort of the mission.

This limitation of classical control, together with need for more safety and lower flight control system development, has sparked interest in research on modern control theories which could cope with the nonlinear behaviour of the aircraft motion [4, 6, 7]. Some examples of these theories are Nonlinear Dynamic Inversion (NDI) and Backstepping [4, 8]. These theories have been applied in several research projects, which demonstrated good performance properties. [9–12]. However, further research on performance sensitivity has established that mismatches in the used on-board model and measurement error lead to considerable performance degradation [13, 14]. This problem stimulated research on control laws which are less dependent on the aircraft model. One of the proposed solutions is Incremental Nonlinear Dynamic Inversion (INDI) [15].

INDI is of similar nature as NDI. It differs from NDI in the sense that the model equations are transformed into linear incremental equations before performing the inversion. Furthermore, assuming that the sampling frequency of the control system is high enough, it is possible to neglect the incremental state dependency of the linearized model. As a result, the model dependency of INDI control laws is significantly reduced. However, this comes at the expense of requiring feedback of the time derivative of the controlled variable, which can be difficult to obtain accurately [14, 15]. Moreover, as a consequence of the incremental model equations, this control law determines the desired incremental control effector change. Therefore, feedback of effector position should be available as well.

The performance of the INDI control law has been demonstrated in past research in several flight test campaigns on platforms such as the VAAC Harrier [16], micro aerial vehicles (MAVs) [17] and the PH-LAB Cessna Citation II of the Delft University of Technology and the Royal Netherlands Aerospace Centre (NLR) [18–20]. Furthermore, it has been theoretically proven that INDI control laws are more robust to parametric system variations and have better disturbance rejection capabilities than their traditional NDI equivalents if the sampling frequency is high enough [21]. Still, MAV flight tests have demonstrated that an INDI flight control law, despite having high sampling rates, may still suffer from performance degradations due to control effectiveness model mismatches [17]. Similar conclusions were also drawn based on stability and performance robustness studies of an INDI-based flight control law for a multi-rotor UAV presented by Gong et al. [22].

In this paper, possible performance variations of INDI-based control laws due to system uncertainties will be examined in the context of handling qualities and stability (HQ&S) guidelines for high-performance (Class IV) aircraft [23]. HQ&S guidelines are developed to predict whether pilot workload will be acceptable during a mission or if the mission can be completed at all [24]. Next to compliance to these guidelines, it is preferred that the variation of the HQ&S remains small despite possible system uncertainties in order to maintain constant predicted pilot workload levels.

Results presented in this paper will show that HQ&S variation due to system uncertainties can occur for an INDI-based pitch rate control law operating at a limited sampling rate (100 Hz). The system uncertainties considered in this paper originate from unanticipated longitudinal centre of gravity (CG) shifts and elevator effectiveness uncertainty. Finally, to cope with these uncertainties, an indirect adaptive control solution based on online system identification and correction of the control effectiveness (CE) model will be investigated. The hypothesis is that an accurate CE model could improve performance robustness against aforementioned issues. The online system identification algorithm used

in this study is based on Least-Mean-Square (LMS) parameter estimation [25, 26], which was also used in [17].

The outline of the paper is as follows. First, the INDI pitch rate control law and the additional online system identification algorithm derivation are described in Section II. This is followed by Section III, which elaborates on the employed design strategy to select the appropriate values for the design parameters of the INDI control law and LMS estimation algorithm. Furthermore, this Section discusses the approach to assess the HQ sensitivity of both the non-adaptive and adaptive pitch rate control law. Section IV clarifies the details of the simulation model used to perform the analysis. Then, the results are presented and discussed in Section V. Finally, the paper is concluded in Section VI.

II. Adaptive Incremental Nonlinear Dynamic Inversion pitch rate control

The control objective considered in this study is to track pilot pitch rate commands. This Section will elaborate on the derivation of the control law architecture using the INDI design framework. Furthermore, the online parameter estimation algorithm based on LMS is treated as well.

A. Inversion loop

As a starting point for the derivation of an INDI-based pitch rate controller, consider the following model for the longitudinal rotational motion of an aircraft that is symmetric about the x-z plane [27]:

$$\dot{q} = \frac{I_{zz} - I_{xx}}{I_{yy}} pr + \frac{I_{xz}}{I_{yy}} \left(r^2 - p^2 \right) + \frac{1}{I_{yy}} \mathcal{M} \tag{1}$$

Linearizing this equation with respect to the current time step, '0', and assuming that the control sampling rate is high enough such that assuming time-scale separation between the control input and incremental state dependent parts is justified [15], the following result can be found:

$$\dot{q} = \dot{q}_0 + \frac{1}{I_{yy}} \frac{\partial \mathcal{M} \left(\boldsymbol{x}_0, \boldsymbol{u}_0 \right)}{\partial \boldsymbol{u}} \Delta \boldsymbol{u} = \dot{q}_0 + \frac{\bar{q}_0 S \bar{c}}{I_{yy}} C_{m_{\delta_e}} \left(\boldsymbol{x}_0, \boldsymbol{u}_0 \right) \Delta \delta_e = \dot{q}_0 + G_0 \Delta \delta_e \tag{2}$$

Setting $\dot{q}$ as the virtual control input, ν_q, and solving for the incremental elevator deflection, $\Delta \delta_e$, Equation (3) is obtained.

$$\Delta \delta_{e_c} = G_0^{-1} \left(\nu_q - \dot{q}_0 \right) \tag{3}$$

Calculating the virtual control input, ν_q, is performed by the outer loop and will be discussed in the next Section. Lastly, to complete the inversion loop the incremental elevator deflection should be added to an elevator deflection feedback signal to obtain the new commanded elevator deflection:

$$\delta_{e_c} = \delta_{e,0} + \Delta \delta_{e_c} \tag{4}$$

B. Outer loop

The architecture of the outer loop consists of a command filter and a closed loop Proportional-Integrator (PI) compensator, as shown in Figure 2. A command filter is applied to directly incorporate the desired aircraft response in a transparent manner and the PI compensator is used to construct a closed loop controller which accurately follows the command filter output and is robust to system uncertainties. The command filter has the following structure:

$$\frac{q_{cf}}{q_{plt}} = \frac{K_{cf_1} s + K_{cf_3}}{s^2 + K_{cf_2} s + K_{cf_3}} \tag{5}$$

This second order command filter architecture has been selected as it has the same structure as the aircraft short period *lower order equivalent system* (LOES) model without time delay [23]. If the control law could accurately follow the command filter output, this control law architecture allows for convenient incorporation of desired second order short term behaviour. This architecture will result in sufficient design flexibility, as will be seen later on. To calculate the virtual control input, a feed-forward term containing the time derivative of the command filter output is added as well. This term is added to assure that the closed loop control tracks the command filter with zero error (in absence of external disturbances) and results in the following control law:

$$\nu_q = K_P \left(q_{cf} - q_0 \right) + \frac{K_I}{s} \left(q_{cf} - q_0 \right) + s q_{cf} \tag{6}$$

3

Consequently, the aircraft tracking response, assuming negligible actuator and feedback path dynamics and perfect inversion, will be as follows:

$$q = \frac{1}{s} v_q = \frac{1}{s} \left(K_P \left(q_{cf} - q_0 \right) + \frac{K_I}{s} \left(q_{cf} - q_0 \right) + s q_{cf} \right) \tag{7}$$

$$\downarrow$$

$$s q + K_p q + \frac{K_I}{s} q = s q_{cf} + K_p q_{cf} + \frac{K_I}{s} q_{cf} \tag{8}$$

$$\downarrow$$

$$\frac{q}{q_{cf}} = 1 \tag{9}$$

Furthermore, using the same assumptions, the ideal nominal response of the control law for a constant command to an error in the pitch rate, $e = q - q_{cf}$, is as follows:

$$\dot{e}(t) + K_p e(t) + K_I \int_0^t e(t) \, dt = 0 \tag{10}$$

C. Least-Mean-Square online parameter estimation

The goal of the online parameter estimation module is to correct for the uncertainty in the on-board control effectiveness model used in the inversion loop. Considering Equation (3), the model uncertainty can be found in the term G_0^{-1}, which depends on the uncertain nonlinear aerodynamic model, $C_{m_{\delta_e}}$, and the mass moment of inertia around the body reference frame Y-axis, I_{yy}, as shown in Equation (2). Both the aerodynamic model and inertia are affected by CG shifts. Furthermore, as the CE is dependent on the aerodynamic model divided by the inertia, the influence of CG shifts on the CE is likely to be nonlinear. To estimate the changes of the inertia and aerodynamic model separately, nonlinear parameter estimation algorithms are required as this model is non linear-in-the-parameters [28]. As these algorithms are rarely suitable for real-time applications, this study will apply another strategy.

The approach applied in this study is to model the uncertainty as lumped together in one uncertain term, $g(\boldsymbol{x}_0, \boldsymbol{u}_0) = I_{yy}^{-1} C_{m_{\delta_e}}(\boldsymbol{x}_0, \boldsymbol{u}_0)$, and estimate online a correction factor, $\hat{C}$, to scale the deviating model until it closely approximates the actual CE of the aircraft. Using this strategy allows for the application of linear parameter estimation methods which have the potential of real-time operation.

The estimation algorithm applied in this study is based on LMS parameter estimation [25, 26]. Algorithms based on this theory have been applied in many adaptive filter applications and has been used before in the control of a UAV [17]. The attractiveness of this approach lies in the straightforward design and the low computational complexity while still being able to obtain accurate estimations [25].

To apply the LMS parameter estimation algorithm for estimating the correction factor, the regression model for the uncertain pitching motion will be written as

$$\dot{q} - \dot{q}_0 = \Delta \dot{q} = \hat{C} \bar{q}_0 S \bar{c} g_{nom}(\boldsymbol{x}_0, \boldsymbol{u}_0) \Delta \delta_e = \hat{C} G_{nom}(\boldsymbol{x}_0, \boldsymbol{u}_0) \Delta \delta_e \triangleq \hat{C} \phi(\boldsymbol{x}_0, \boldsymbol{u}_0) \tag{11}$$

Here, $\phi(\boldsymbol{x}_0, \boldsymbol{u}_0)$ is the regression model basis function and contains the nominal CE model, $G_{nom}(\boldsymbol{x}_0, \boldsymbol{u}_0)$, that predicts the nominal increment of $\dot{q}$ from an increment in δ_e. Consequently, the LMS parameter estimation algorithm is shown in Equation (12).

$$\hat{C} = \hat{C}_0 + \mu \phi(\boldsymbol{x}_0, \boldsymbol{u}_0) \left(\Delta \dot{q} - \hat{C}_0 \phi(\boldsymbol{x}_0, \boldsymbol{u}_0) \right) \tag{12}$$

The estimated value of the required correction factor, $\hat{C}$, will be used to improve the control effectiveness model used for inversion by the INDI control law. Consequently, the inversion loop of the LMS adaptive INDI pitch rate control law has the following structure:

$$\Delta \delta_e = \left(\hat{C} G_{0,nom} \right)^{-1} \left(v_q - \dot{q}_0 \right) \tag{13}$$

4

III. Control law design and evaluation strategy

This Section elaborates on the search for appropriate control law design parameters and the strategy to evaluate the HQ&S sensitivity of the non-adaptive and adaptive control laws. As the adaptive control law can be considered as a non-adaptive control law with a modular adaptive element, the design phase will consist of two parts. Section III.A focuses on the selection of the parameters for the non-adaptive control, $K_p, K_I, K_{c f_1}, K_{c f_2}, K_{c f_3}$, and Section III.B treats the selection of the appropriate LMS adaption gain, μ. Lastly, Section III.C treats the HQ&S evaluation approach adopted in this study.

A. Non-adaptive control law design

The goal of this study is to analyse whether online correction of the on-board CE model could decrease the sensitivity of the HQs and control performance. To achieve this objective, the non-adaptive control law will be designed taking into account relevant HQ guidelines during the development process. This approach allows for improved realism of the design and therefore the final sensitivity results are easier to put into a practical perspective.

To be able to perform this design approach, the student version (6.0) of the software package CONDUIT® is utilized [29]. This software package allows for optimization of the control law design parameters while immediately reflecting the intermediate design iterations on the considered HQ&S specifications. However, the student version itself contains a restricted amount of specifications. Therefore, to be able to perform the optimization and analysis, several are custom made using Specmaker version 1.5 [29]. These specifications are indicated with a '*' in Table 1 and 2.

Resources for relevant HQ guidelines are the military standards MIL-STD-1797A [23] and several other handling quality technical reports and best practices [29–34]. From these sources a set of handling quality guidelines as listed in Table 1 is selected. The selected design guidelines are considered important for design and verification of longitudinal control laws of high-performance aircraft. In this view, the goal of the design phase is to find a set of parameters for which all considered handling quality and stability characteristics are inside the specified Level 1 regions.

Furthermore, to guide the optimization, several extra design objectives are added to the optimization. These additional objectives are summarized in Table 2. The goals of these objectives are to monitor the design process and ensure that the control law remains stable and the broken-loop response remains robust for shifts in gain/phase margins, and are included in the first three rows of Table 2. Furthermore, additional objectives for the LOES guidelines and command model following performance are applied to improve the second order behaviour of the closed-loop controlled aircraft (row 4 and 5 of Table 2). Lastly, the actuator activity is monitored for the pilot and disturbance input and the broken-loop cross-over frequency is evaluated.

It should be noted that it is generally recommended [29] to minimize the actuator activity to find a baseline design that satisfies all objectives while using the least amount of control power possible. This approach reduces actuator wear and the chance of Pilot Induced Oscillations (PIO). Furthermore, starting from this baseline design, Tischler [29] advises to perform a design margin optimization by increasing the minimum cross-over frequency requirement in several steps. This approach results in a set of designs on a Pareto optimum front, from which the most desirable option can be selected. However, a different approach will be followed in this study, as the control law will be optimized directly for maximal performance robustness. This robustness will be induced by maximizing the broken-loop cross-over frequency at the broken-loop location, which is at the input of the actuators as shown in Figure 1, while keeping the other requirements in their Level 1 regions. Approaching the control problem in this manner allows for as much control bandwidth as possible to overcome uncertainties associated with parametric system variations. However, increasing the performance robustness does come at the cost of decreasing stability robustness against unmodeled high-frequency parasitic dynamics [36, 37]. Consequently, there is always an upper limit for the achievable performance robustness in practice. However, in this study, this type of parasitic dynamics will not be considered. Therefore, the proposed design strategy is regarded appropriate to illuminate the additional performance robustness benefits provided by the adaptive module.

Although the INDI control design framework allows for nonlinear control law design due to the inclusion of the nonlinear CE model of the aircraft, the HQ guidelines used for the control law design here are developed for linear control systems. Consequently, the control law design and evaluation could only be performed for linear systems, which means that this process should be performed separately for a trimmed and linearized control system at each considered flight condition.

B. LMS parameter estimation algorithm design

The design phase of the LMS estimation algorithm consists of selecting an appropriate value for the adaption gain, μ. This will be done by evaluating the estimation performance during time-domain simulations for different adaption

Table 1 Handling quality criteria for optimization.

Criterion Name	Description	Source	Comment
Short Period damping (ζ_{SP}) vs. Control Anticipation Parameter (CAP)*	Restrains CAP and LOES ζ_{SP}.	MIL-HDBK-1797A [23]	Simultaneous short term pitch rate and load factor response fit. 0.1-10 rad/s.
Equivalent Time Delay*	Evaluates the LOES fit equivalent time delay.	MIL-HDBK-1797A [23]	Simultaneous short term pitch rate and load factor response fit. 0.1-10 rad/s.
Pitch attitude Dropback*	PIO guideline. Restrains the pitch rate overshoot and pitch attitude dropback.	WL-TR-94-3162 [31]	Pitch rate unit step input held for 8 seconds.
Neal-Smith*	Evaluates pilot effort for pilot-in-the-loop closed-loop pitch attitude control.	MIL-HDBK-1797A [23] AFFDL-TR-70-74 [35]	Pilot model settings: ω_{BW} = 3.5 rad/s, T_{lag} = 0.25 s, Max. droop = -3 dB. 0.1-10 rad/s.
Pitch attitude bandwidth vs. Phase delay*	PIO guideline. Limits the pitch attitude bandwidth and phase delay.	WL-TR-94-3162 [31]	0.1 - 50 rad/s.
Gibson Phase Rate*	PIO guideline. Limits the phase rate at $\omega_{\phi=180^o}$ and limits $\omega_{\phi=180^o}$.	AGARD-CP-508 [32]	0.1 - 50 rad/s.
Flight Path Bandwidth vs. Pitch Attitude Bandwidth*	Ensures appropriate ratio of flight-path and pitch attitude bandwidth.	WL-TR-94-3162 [31]	0.1 - 50 rad/s.

* Indicates a custom criterion developed in CONDUIT® Specmaker 1.5.

gain values. The metrics used for the performance characterization are the Root-mean-square (RMS) [14, 38] and $\mathcal{L}_\infty$-norm [39–41] of the temporal error between the actual CE and the corrected CE model, and the cumulative moving standard deviation (CMSD) of the estimated correction factor, $\hat{C}$ [42]. The mathematical descriptions of these metrics are defined as described in Equations (14) until (16).

$$RMS\left(e_G\right) = \sqrt{\frac{1}{N}\sum_{i=1}^{N}\left(\hat{C}\left(i\right)G_{nom}\left(i\right) - G\left(i\right)\right)^2} \tag{14}$$

$$\|e_G\|_\infty = \max_{t\in T}\left\{\left|\hat{C}\left(t\right)G_{nom}\left(t\right) - G\left(t\right)\right|\right\} \tag{15}$$

$$CMSD\left(\hat{C}\right) = \sum_{j=n_s/2+1}^{N-n_s/2}\sqrt{\frac{1}{n_s - 1}\sum_{k=0}^{n_s-1}s_j\left[k\right]}, \quad s_j\left[k\right] = \left(\hat{C}\left[j - n_s/2 + k\right] - \bar{\hat{C}}_j\right)^2 \tag{16}$$

Here, G_{nom} is the nominal on-board model used by the INDI-based pitch control law. Furthermore, s_j and $\bar{\hat{C}}_j$ are the local variance and average estimated correction factor of the data window, respectively. The RMS of the estimation history is used as metric for the spread in the error or constant bias during the simulation. Besides, as the amount of simulation time is limited, a smaller RMS value also could indicate that the parameter estimation converges close to the desired value faster. Furthermore, the $\mathcal{L}_\infty$-norm of the estimation error gives the maximum observed error value during the simulation. This metric shows whether the parameter estimation remains bounded during the simulation and could be used to analyse how this bound changes for different values of the adaption gain. Lastly, the CMSD of the estimated parameter gives an indication of the estimation activity during the simulation. A high value means that the estimated parameter still experiences significant variation despite being converged around a mean value. Too much variation is

Table 2 Additional criteria for optimization.

Criterion Name	Description	Source	Comment
Eigenvalues	Ensures stable eigenvalues of control system.	Practical Methods for Aircraft and Rotorcraft Flight Control Design [29]	Max. real value: 10^{-3}.
Nichols Margins (Broken-Loop)	Ensures robustness for simultaneous shifts in broken-loop gain/phase margins	FM(AG08)-TP-088-4 [43]	0.01 - 100 rad/s. Loop broken before actuator input
Gain/Phase Margins (Broken-Loop)	Ensures robustness in broken-loop gain and phase margin	MIL-DTL-9490E [44]	0.01 - 100 rad/s. Loop broken before actuator input.
Max. Allowable LOES Cost	Limits the LOES fitting cost.	MIL-HDBK-1797A [23]	Limit set at 20. MUAD bounds are driving limits.
Model Following Cost*	Ensures closed-loop control law accurately follows the command filter output.	Practical Methods for Aircraft and Rotorcraft Flight Control Design [29]	Uses LOES equi. time delay. Simultaneous short term pitch rate and load factor response fit. 0.1 - 10 rad/s.
Actuator RMS (pilot input)	Evaluates RMS actuator position. Measure for actuator activity.	Practical Methods for Aircraft and Rotorcraft Flight Control Design [29]	0.1 - 1000 rad/s. Max. pilot input: 20 deg/s. Max. actuator deflection 25 deg.
Actuator RMS (disturbance input)	Evaluates RMS actuator position. Measure for actuator activity.	Practical Methods for Aircraft and Rotorcraft Flight Control Design [29]	0.1 - 1000 rad/s. Max. disturbance input 10 deg/s. Max. actuator deflection 25 deg.
Cross-over frequency (Broken-Loop)	Evaluates the broken-loop cross-over frequency	Practical Methods for Aircraft and Rotorcraft Flight Control Design [29]	0.1 - 40 rad/s. Loop broken before actuator input.

* Indicates a custom criterion developed in CONDUIT® Specmaker 1.5.

unwanted as this could affect the control performance of the complete adaptive control law again. Consequently, the value of the adaption gain will be selected such that the CMSD will be as low as possible.

The variation of these performance metrics will be analyzed for different values of the adaption gain for all deviation cases described in Section III.C. Considering the variation, an adaption gain will be selected for which the LMS parameter estimation achieves adequate performance according to the three metrics described above.

C. Handling quality sensitivity evaluation

This Section will discuss process of the HQ&S sensitivity analysis. A practical approach is adopted in which different CG locations together with CE uncertainty will be considered. The CG cases will be simulated depending on the fuel distribution in the aircraft. As will be shown in Section IV.B, a fuel tank configuration consisting of one front and one rear tank will be assumed. Furthermore, using this configuration, the handling qualities and stability for the nominal, most forward, most aft and a low fuel CG locations will be analysed. In addition, an elevator effectiveness deviation of -15%, 0% and +15% will be applied at each CG location. This means that a total of twelve cases will be evaluated. From these cases the one with a nominal CG position and 0% CE deviation will be used for the nominal control law design. Moreover, these cases will be analysed for different flight conditions to be able to evaluate the efficacy of the online parameter estimation at different points in the flight envelope. The considered flight conditions in

Table 3   Flight condition information.

|		FC-1	FC-2	FC-3	FC-4
Altitude	[m]	12000	3000	7000	5000
Mach number	[-]	0.6	0.6	0.4	0.5
Velocity	[m/s]	177	197	125	160
Dynamic pressure	[Pa]	4871	17667	4599	9453

this study are described in Table 3.

To analyse the handling qualities and stability for each case, the CONDUIT® software package will be used. For the analysis of the non-adaptive control law, only the aircraft model will change according to the considered deviations. Therefore, the change in HQs will be determined using the nominal control law design.

Determining the HQs sensitivity of the adaptive control law will require a combination of time-domain simulations and HQ&S determination using CONDUIT®. The time-domain simulations will be performed with the non-linear aircraft model to verify that the parameter estimation would still function with the complete system dynamics. During the simulations, the adaptive control law will execute a pitch rate tracking task and the parameter estimator will attempt to find the optimal correction factor. The tracking task will be repeated several times, each time starting with the last estimated value of the correction factor from the previous simulation. Each repetition of the tracking task is called an episode. The tracking task will be repeated until the estimation response does not show significant differences between simulations anymore. At this point convergence is achieved and the average value of the correction factor estimation response will be used for the HQs evaluation. The CE model used in the non-adaptive control law will be multiplied by this average value and the HQ&S are re-evaluated.

IV. F-16 aircraft model

The high-performance aircraft model which will be used in this study is an open-source General Dynamics F-16 model developed by [37, 45, 46]. The aerodynamic database used in this aircraft model is obtained from low-speed wind-tunnel tests and is claimed to be valid for control system design up to about Mach 0.6 [45]. A reduced version of this model described by Stevens and Lewis [37, 46] is used, which is valid for an angle-of-attack range of $-10 \leq \alpha \leq 45$ degrees and sideslip angles of $|\beta| \leq 30$ degrees. To be able to carry out the analysis steps described in the preceding sections, some modifications have been made to the standard simulation model. This will be further elaborated on in this Section. Figures 1 and 2 respectively present the block schemes of the inversion loop and outer loop containing all components described in this Section.
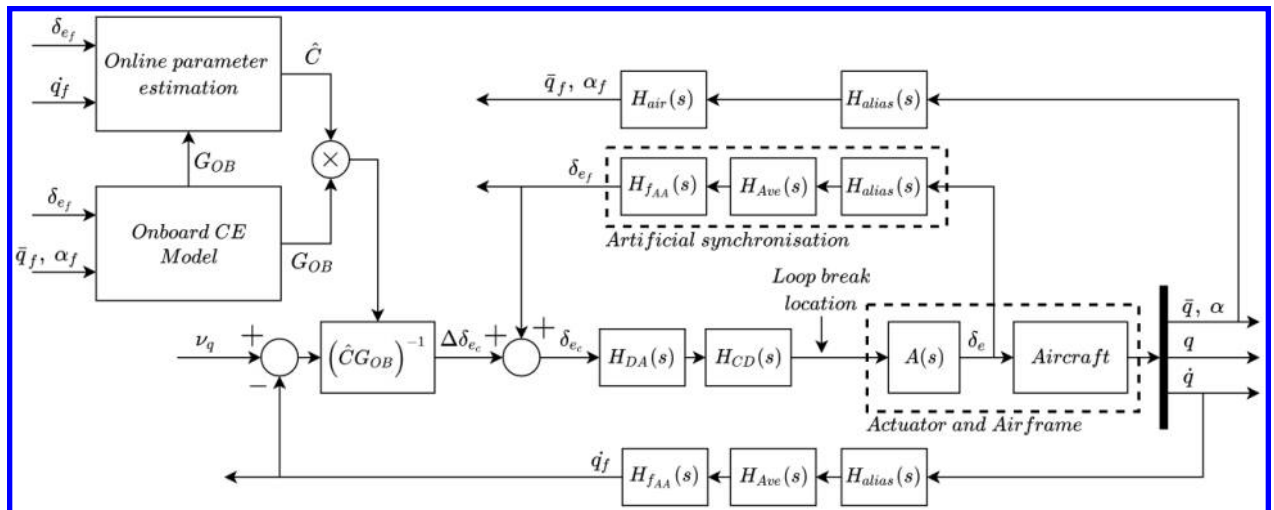
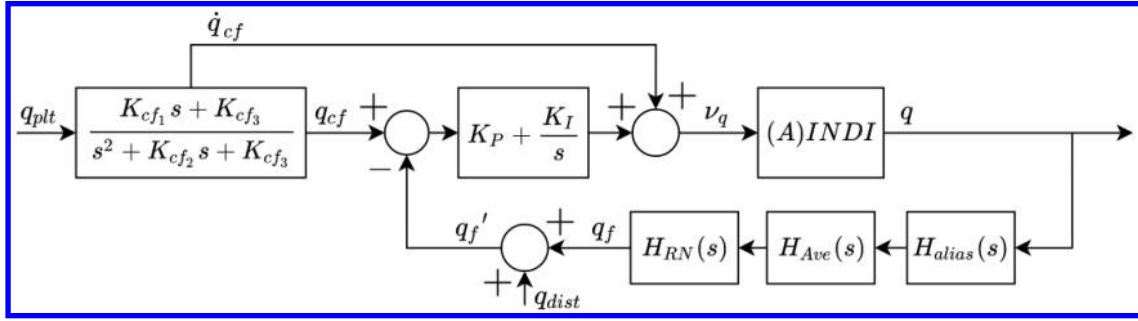**Fig. 1   Adaptive INDI control system inner loop block scheme including broken-loop location.**

8

Fig. 2 Adaptive INDI control system outer loop block scheme including pitch rate disturbance input location.

A. Control System Properties

Real-world fly-by-wire (FBW) control systems are not ideal due to the presence of additional dynamics introduced by sensors, filters and actuators. The derivation of an INDI-based control law assumes instantaneous deflections of the elevator and no loss of information of the feedback signals. As these characteristics cannot be achieved in real-world systems, the control performance and stability will be decreased with respect to an ideal system. Furthermore, as noise is always present, filters are implemented as well, which affects the feedback signals. Consequently, to improve the fidelity level of the analysis, these aspects are also taken into account. The models used here are taken from the GARTEUR High Incidence Research Model (HIRM) benchmark model described by Muir [43], for the reason that the GARTEUR HIRM benchmark challenge focused on the flight control system design task of a similar high-performance aircraft and provides a clear description of the system elements. The sensor dynamics are specified for air data, and rate and linear accelerations:

- Air data:

$$H_{air}(s) = \frac{1}{0.02s + 1} \tag{17}$$

- Rate and linear acceleration (with notch filter):

$$H_{RN}(s) = \frac{0.0001903s^2 - 0.005346s + 1}{0.0004942s^2 + 0.03082s + 1} \tag{18}$$

Furthermore, for this control system it is assumed that the pitch acceleration can be measured directly using an angular accelerometer (AA) [19]. The dynamics of this feedback signal is presumed to be mostly dominated by the filter dynamics. The filter structure used for the angular acceleration measurements is the same as used in [19]:

$$H_{f_{AA}}(s) = \frac{\omega_{f_{AA}}^2}{s^2 + 2\zeta_{f_{AA}}\omega_{f_{AA}}s + \omega_{f_{AA}}^2} \tag{19}$$

The filter parameters are set as $\omega_{f_{AA}} = 30$ rad/s and $\zeta_{f_{AA}} = 1$. Furthermore, for incremental control laws it has been observed that synchronization of the angular acceleration and control surface deflection is necessary. For this analyses, the same approach as used in Smeur et al. [17] will be adopted. Consequently. the synchronization of these signals is achieved by delaying the elevator deflection measurement using an equivalent filter which approximates the angular acceleration feedback dynamics. A more advanced approach could involve real-time estimation of the relative delay, as described by van 't Veld et al. [47], but this will not be considered in this study. In addition to these models, Muir [43] specifies that the rate and linear acceleration feedback paths also contain averaging dynamics and that these can be modelled as zero-order-hold (ZOH), see Equation (20). Next to these channels it will be assumed that averaging will also be required for the angular acceleration feedback signal.

Next to the feedback dynamics described by [43], the complete control system model will also account for a limited sampling frequency of the system. This is added to the model as modern FBW control systems are of digital nature. It is assumed that the system in this study operates at 100 Hz. To incorporate the limitations of the restricted sampling rate, continuous-time models of anti-aliasing, $H_{alias}(s)$, a digital-to-analogue (DA) converter, $H_{DA}(s)$, and computational delay, $H_{CD}(s)$, are added to the simulation model [37]. The delay, assumed to be one sampling period, is implemented

9

just before the actuator input and is modelled using a second order Padé approximant. Furthermore, the anti-aliasing filters are placed just after the sensor models. The DA converter will be modelled as a continuous-time ZOH transfer function and the anti-aliasing as a first order lag with the cut-off frequency less than half the sampling frequency, here selected at 45 Hz [37]:

$$H_{DA}(s) = \frac{\frac{T_s^2}{60}s^2 - \frac{T_s}{10}s + 1}{\frac{T_s^2}{20}s^2 + \frac{2T_s}{5}s + 1} \tag{20}$$

$$H_{alias}(s) = \frac{\omega_{alias}}{s + \omega_{alias}} \tag{21}$$

The block diagrams describing the complete control system are shown is Figures 1 and 2.

B. Mass model

Handling quality analysis will be performed for different CG locations. These CG locations are obtained by changing the fuel distribution over the tanks. To be able to do this a geometric configuration of one front and one rear fuel tank will be assumed. According to the US Air Force official website*, the total fuel capacity of the F-16C/D, without external tanks, is approximately 3175 kg and the aircraft empty mass is approximately 8936 kg. The parameters used for the mass model are shown in Table 4 and the equations used to determine the CG shifts are given in Equations (22) and (23). In this model it is assumed that the mass moment of inertia of the fuel in the tank itself can be neglected and therefore only the parallel axis term is applied.

Table 4   Mass model parameters.

		Front tank (ft)	Rear tank (rt)	Airframe (af)
Longitudinal CG position (x_{cg})	[$\bar{c}$]	-0.3	0.9	0.35
Capacity (C) / Mass (M)	[kg]	1587.5	1587.5	8936
Inertia (I)	[kg·m^2]	-	-	74121

$$x_{cg,tot} = \frac{x_{cg,af}M_{af} + x_{cg,ft}C_{ft} + x_{cg,rt}C_{rt}}{M_{tot}} \tag{22}$$

$$I_{yy,tot} = I_{yy,af} + M_{af}\bar{c}^2\left(x_{cg,af} - x_{cg,tot}\right)^2 + C_{ft}\bar{c}^2\left(x_{cg,ft} - x_{cg,tot}\right)^2 + C_{rt}\bar{c}^2\left(x_{cg,rt} - x_{cg,tot}\right)^2 \tag{23}$$

To be able to use the values for the different CG location, inertia and total mass, the University of Minnesota F-16 Simulink model inputs have been adjusted such that these quantities could serve as model input as well. The mass and inertia properties of the aircraft at the nominal (nom), forward (fwd), aft and low-fuel (LF) CG locations are summarized in Table 5.

Table 5   Mass and inertia properties per CG location.

		Nominal	Forward	aft	Low fuel
Longitudinal CG position ($x_{cg,tot}$)	[$\bar{c}$]	0.338	0.254	0.435	0.350
Total mass (M_{tot})	[kg]	12111	10523	10523	9253
Inertia ($I_{yy,tot}$)	[kg·m^2]	87804	80944	78941	75492

---

*USAF, 'F-16 Fighting Falcon', *US Air Force*, Hampton, USAF, 2015, https://www.af.mil/About-Us/Fact-Sheets/Display/Article/104505/f-16-fighting-falcon/, (accessed December 10, 2020)

V. Results and discussion

The simulation and analysis results will be shown and discussed here. First, the control law designs for each flight condition will be discussed in Section V.A. It should be noted that during the analysis, it was found that the results of FC-1 were quite similar to those of FC-3, whereas the results of FC-4 showed significant resemblance to FC-2. Therefore, to focus on the most relevant results, Section V.B will only display the HQ&S results of FC-2 and FC-3. Lastly, the presented results will be discussed more elaborately is Section V.C.

The analysis of the parameter estimation is performed in the time domain. Consequently, it is required to define a standard pitch rate tracking signal. This signal is shown in Figure 3 and was constructed such that the aircraft motion remains inside the linear region of the flight condition.
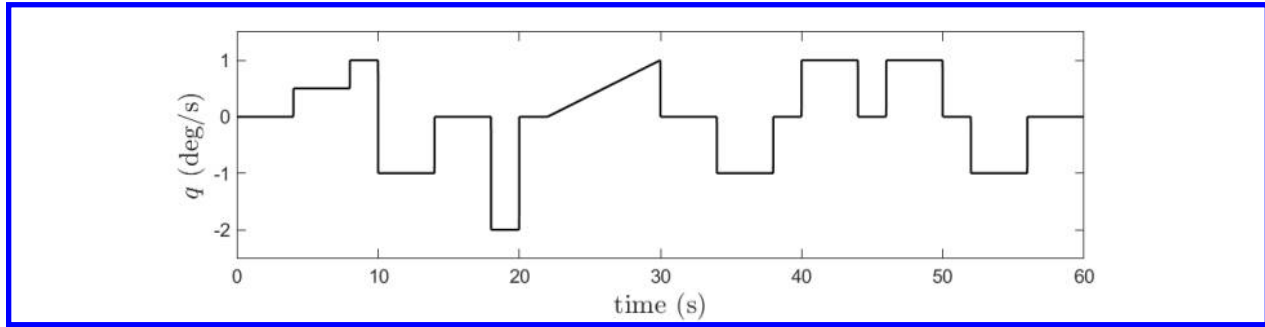
Fig. 3   Pitch rate tracking signal

A. Control law design results

After linearizing the nonlinear F-16 model at the trim conditions and nominal CG location described in tables 3 and 5 , respectively, the the control law design parameters were optimized next. The initial parameter values and their final optimized results are shown in Table 6. Shaping the initial parameter values of the command filter is based on placing the desired short period dynamics such that the CAP and ζ_{SP} would be in the centre of the level 1 region of the CAP vs. ζ_{SP} requirement. This design point corresponds to a CAP of 1 and a ζ_{SP} of 0.7. To achieve this, the zero of the aircraft short period transfer function is used. Furthermore, the initial PI compensator gains are manually selected such that the control law follows the command model with reasonable accuracy. For all flight conditions, this holds for initial proportional and integral gains of 4.00 and 1.00, respectively. Lastly, all final designs shown in Table 6 achieved the Level 1 regions of the requirements. However, it was found that the CAP vs. short period damping, the attitude dropback and the Neal-Smith were often competing requirements and therefore ended on the boundary of the Level 1 region. To comply with these requirements, it was necessary to increase the value of the zero in the command model and often decrease the natural frequency. Depending on the flight condition this leads to an increase in the short period damping or a decrease of the CAP as can be seen in Figures 13 and 15.

To select the appropriate value for the LMS adaption gain, μ, the sensitivity of the parameter estimation performance metrics described in Section III with respect to μ is analyzed for all uncertainty cases. Considering these results, the RMS CE model error and the CMSD of the correction factor estimation were most critical for selecting an appropriate value of μ. Therefore, the trends observed for these metrics are presented in Figures 4-7 and will be briefly discussed.

Table 6   Control law design optimization results.

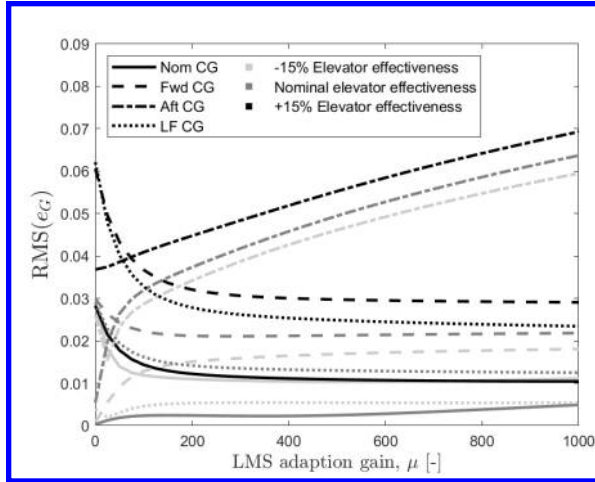|	FC-1		FC-2		FC-3		FC-4	
DP	Initial	Final	Initial	Final	Initial	Final	Initial	Final
K_P	4.00	4.22	4.00	7.07	4.00	3.93	4.00	5.45
K_I	1.00	0.91	1.00	0.00	1.00	1.04	1.00	0.28
K_{cf_1}	18.05	8.29	20.10	6.15	12.74	8.31	16.34	8.02
K_{cf_2}	2.99	3.52	5.43	2.97	2.86	3.29	3.96	2.94
K_{cf_3}	4.57	4.64	15.06	6.55	4.18	5.36	7.98	5.21

11

Fig. 4 RMS of the CE model error as a function of μ for all uncertainty cases at FC-2.
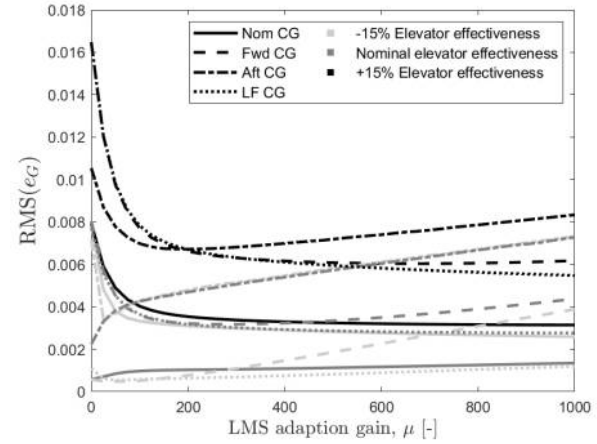
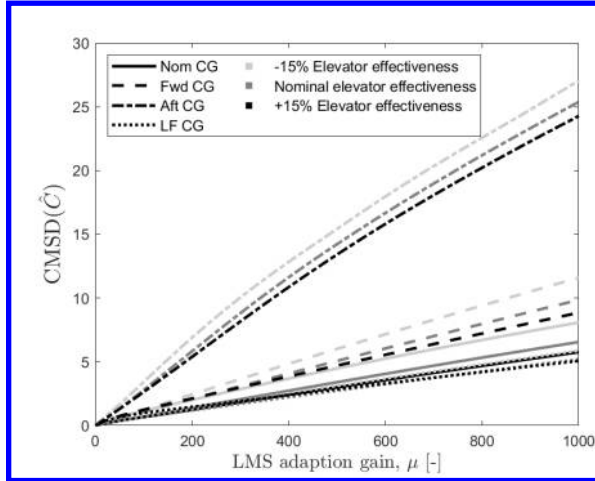**Fig. 5 RMS of the CE model error as a function of μ for all uncertainty cases at FC-3.**

Fig. 6 CMSD of the correction factor estimation as a function of μ for all uncertainty cases at FC-2.
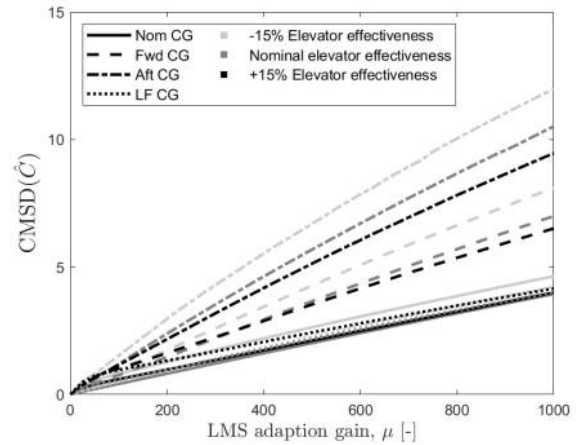
Fig. 7 CMSD of the correction factor estimation as a function of μ for all uncertainty cases at FC-3.

The RMS CE model error shows to have a flattening trend for increasing values of μ for the nominal, forward and low-fuel CG locations. However, for an aft CG location, it is clear that the RMS value starts to rise after a certain value of μ. Considering FC-2, the RMS value even increases for all values of μ. Furthermore, from Figures 6 and 7 it can be seen that the estimation CMSD has a near linear growth with respect to the adaption gain. As explained in Section III.B this value should be as low as possible. Taking into account the increasing RMS value for an aft CG location and the always increasing CMSD, a value of 150 was considered an appropriate choice for μ for all flight conditions.

B. Handling quality sensitivity results

The estimation of the correction factor for FC-2 and FC-3 are shown in Figures 8 until 11. These time responses are obtained for the scenario that the CE model has not been corrected before the start of the first episode. Figures 8 and 10 correspond to the estimation response of the first episode and Figures 9 and 11 to that of the converged episode. The responses result from following the pitch rate reference signal displayed in Figure 3. Considering the estimation results for $\mu = 150$ it was found that approximately 20 seconds are required to reach convergence for all uncertainty cases.
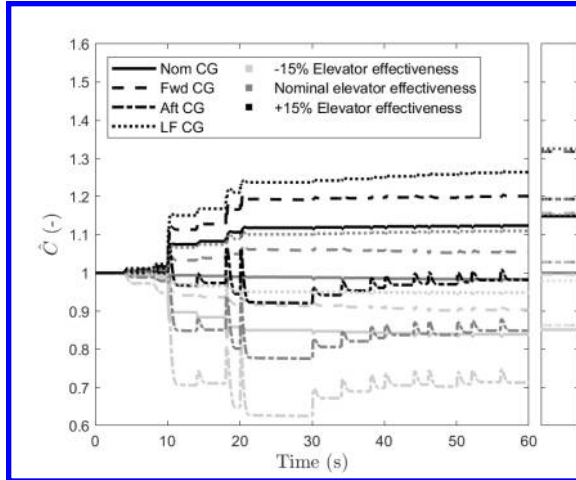
12

Fig. 8   Correction factor estimation over time of all uncertainty cases. First episode for $\mu =$ 150 and FC-2. The desired value is given in the window on the right side.
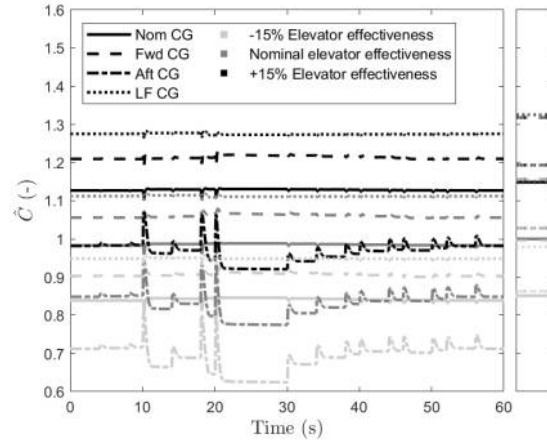
Fig. 9   Correction factor estimation over time of all uncertainty cases. Converged episode for $\mu = 150$ and FC-2. The desired value is given in the window on the right side.
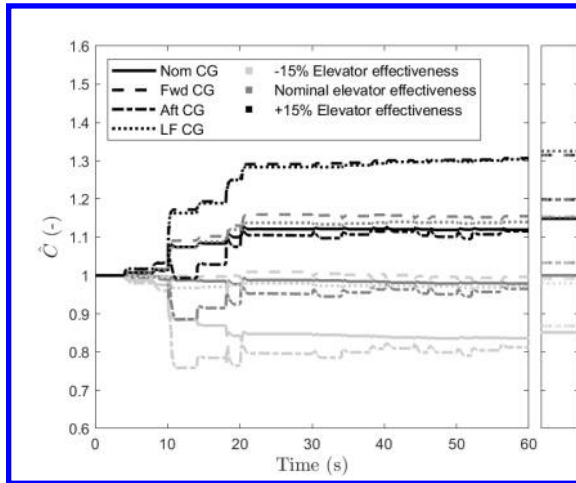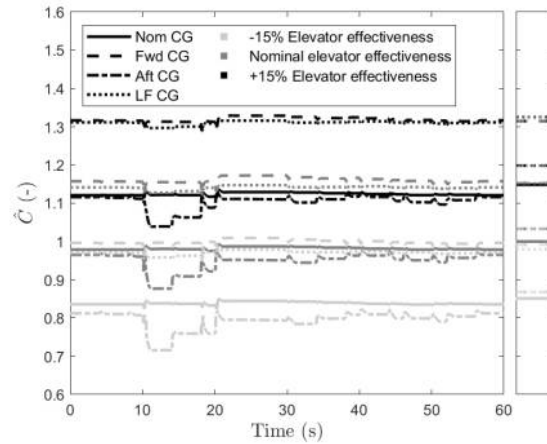
Fig. 10   Correction factor estimation over time of all uncertainty cases. First episode for $\mu =$ 150 and FC-3. The desired value is given in the window on the right side.

Fig. 11   Correction factor estimation over time of all uncertainty cases. Converged episode for $\mu = 150$ and FC-3. The desired value is given in the window on the right side.

As predicted by the sensitivity of the RMS CE model error and the CMSD of the correction factor estimation, the aft CG location parameter estimation shows more activity than the estimation of the other CG locations. Furthermore, taking the average values of the responses of Figures 9 and 11, it can be seen that the parameter estimation for some cases generate quite some underestimations. Despite these results, Figures 12 until 19 clearly show that the sensitivity of the CAP versus short period and the attitude dropback HQ guidelines is decreased for the cases under consideration. These results indicate that the added value of online parameter estimation mainly lies in coping with the CE uncertainty, because the variations due to CG shifts still remain. This is further illustrated by the time response to the first step of the pitch rate tracking signal, as shown in Figures 20 and 21.
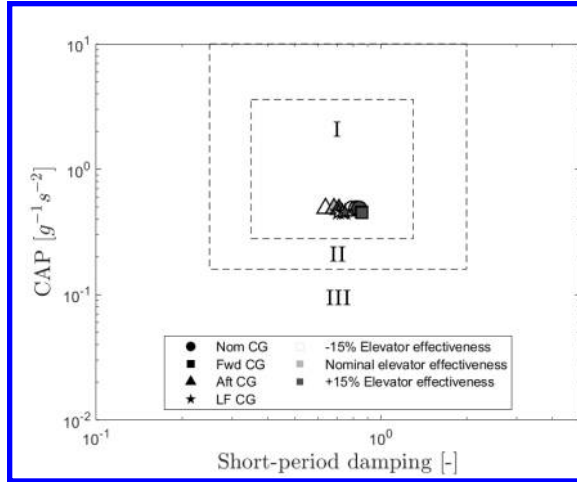
13

Fig. 12   CAP vs. short period damping criterion sensitivity for FC-2 and non-adaptive control
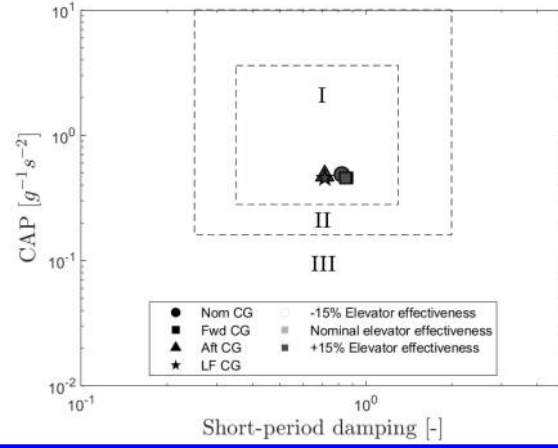
Fig. 13   CAP vs. short period damping criterion sensitivity for FC-2 and adaptive control.
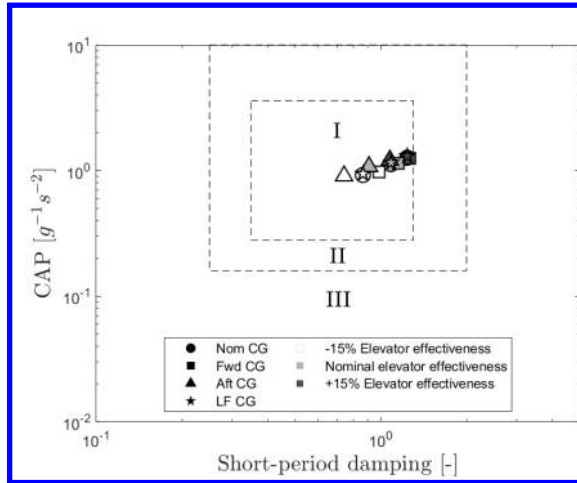

Fig. 14   CAP vs. short period damping criterion sensitivity for FC-3 and non-adaptive control.
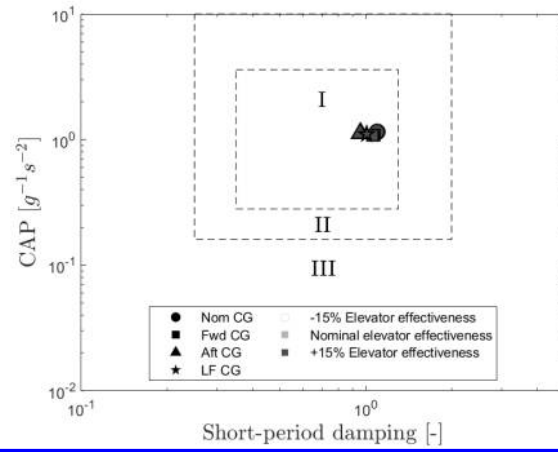
Fig. 15   CAP vs. short period damping criterion sensitivity for FC-3 and adaptive control.

C. Discussion

The results obtained in the previous Section indicate that the addition of online parameter estimation and model correction using LMS leads to a decrease of the variations in HQ&S of the INDI-based pitch rate control law. However, there are some aspects related to the obtained control law designs and parameter estimation which could be further illuminated. First, the optimized PI compensator gains of the non-adaptive INDI pitch rate control law show a significant variation over the different flight conditions. For the design of a proper gain scheduling function, it is desired to have a smooth transition of the control gains for changes in the scheduling variables [29, 48]. Consequently, these gain values might not be the most appropriate choice for use in a gain scheduling controller. However, the purpose of the design was to obtain as much robust performance as possible for each flight condition by finding a set of gains that maximizes the broken-loop cross-over frequency.

In case a smoother scheduling is desired, Sonneveldt [49] describes a scheduling method for the natural frequency of the command filter that is linearly dependent on the dynamic pressure. The command filter natural frequency changes from 2.5 rad/s for low dynamic pressure to 6.5 for high dynamic pressure. Furthermore, Berger [34] describes an approach where all designs are optimized for a single specified cross-over frequency. The optimized control gains are scheduled according to dynamic pressure and Mach number, and do show a smooth transition over the flight domain.
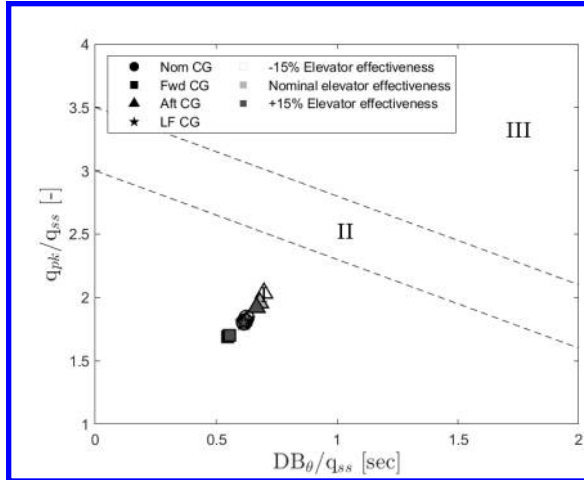
Fig. 16   Pitch attitude dropback criterion sensitivity for FC-2 and non-adaptive control.
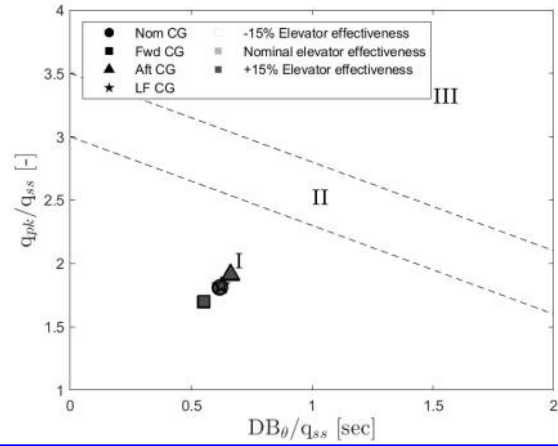
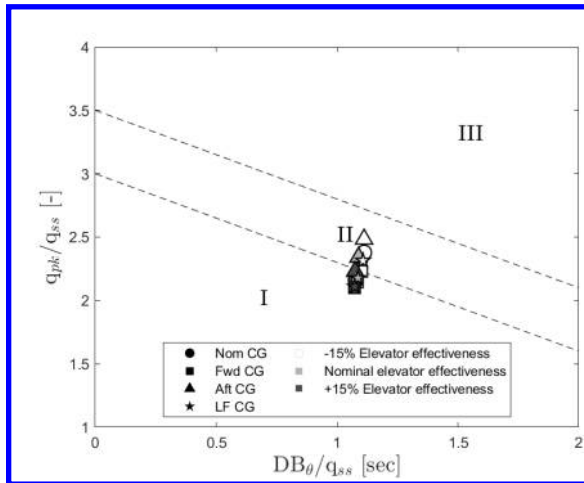**Fig. 17   Pitch attitude dropback criterion sensitivity for FC-2 and adaptive control.**

Fig. 18   Pitch attitude dropback criterion sensitivity for FC-3 and non-adaptive control.
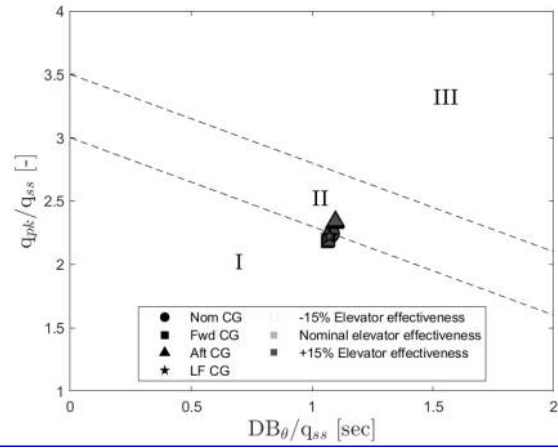
Fig. 19   Pitch attitude dropback criterion sensitivity for FC-3 and adaptive control.

Analyzing the obtained command model natural frequencies of Table 6, it can be seen that the natural frequencies found here behave differently compared to the linear scheduling used by Sonneveldt [49]. Although a similar relation seems to be present between the dynamic pressure and the natural frequency for the initial design parameter values in Table 6, it can be seen that this relation changes considerably after the optimization.

Reconsidering the parameter estimation responses of FC-2 in Figure 9, the estimation of the correction factor for the forward and aft CG cases show larger deviations for the desired value and more activity than the correction factor estimations for same CG cases of FC-3 shown in Figure 11. Furthermore, the average estimation error of the correction factor for an aft CG location and -15% elevator effectiveness at FC-2, is nearly equal to the deviation at the start of the first episode. Despite this significant deviation after convergence, it was observed that the sensitivity of CAP versus short period damping and attitude dropback criteria still decreased, as can be seen Figures 13 and 17. A possible explanation for this lies in the fact that an underestimation of the correction factor is obtained, which is observed multiple times in this study. The consequence of an underestimation is a lower value for the CE model. The successive result of a lower CE value is a larger elevator deflection increment determined by the INDI controller. Although this could result in an overshoot of the optimum elevator deflection, it could also result in a quicker convergence to a desired elevator deflection. Therefore, the lower CE model value could also function slightly like high-gain control for the inversion and induce some performance robustness. However, this comes at the cost of degraded stability properties in case of
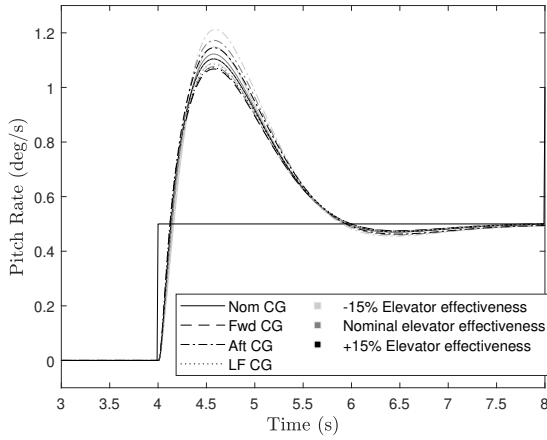
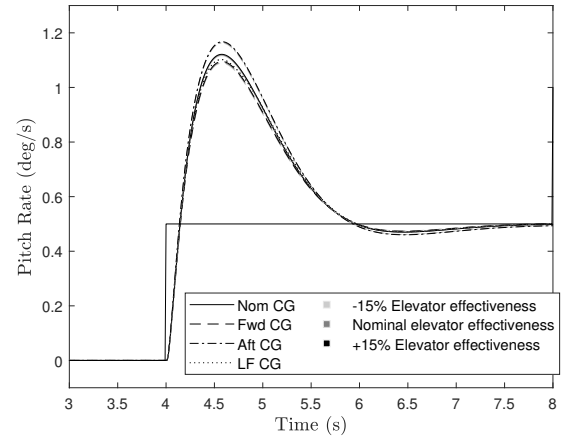**Fig. 20 Pitch rate response of the non-adaptive control law for FC-3.**

Fig. 21 Pitch rate response of the adaptive control law for FC-3.

unmodeled high-frequency parasitic dynamics, as explained earlier in Section III.A.

The question rises what causes the underestimation of the correction factor estimation. Further investigation of the nominal and low-fuel CG locations for both flight conditions in Figures 9 and 11 make clear that these are not as much affected by differences in flight condition as the other CG location cases. Considering that FC-2 is a flight condition with a higher dynamic pressure than FC-3, see Table 3, the problem can be a result of an increased sensitivity of the aerodynamic forces and moments for changes in the aircraft states. This can be confirmed by the linearized $\Delta\dot{q}$ model coefficients shown in Table 7. Especially the model coefficient m_α at FC-2 increases considerably in magnitude for a forward and aft CG shift. The result of this significant increase in influence of $\Delta\alpha$ on $\Delta\dot{q}$ could weaken the assumption that the $\Delta\alpha$ dependency is negligible.

Figures 22 and 23 confirm that the influence of $\Delta\alpha$ on $\Delta\dot{q}$ becomes more dominant when the CG has shifted to the aft location. The response shown in these figures is obtained by tracking the pitch rate ramp segment in the tracking signal of Figure 3 and using the linearized aircraft model at FC-2. Reconsidering Figure 9, the parameter estimation shows the worst performance during this period for an aft CG position. A comparison of Figures 22 and 23 shows that only accounting for the effect of $\Delta\delta_e$ after the initial transient does not give a good description of $\Delta\dot{q}$ for an aft CG location. Consequently, the assumption of neglecting the effects of $\Delta\dot{q}_{\Delta\alpha}$ and $\Delta\dot{q}_{\Delta q}$ does not hold here. This would explain the observed offset in the parameter estimation for the aft and forward CG locations at FC-2.

Although it is expected that the parameter estimation problems can be overcome by adding the estimation of the $\Delta\dot{q}_{\Delta\alpha}$ and $\Delta\dot{q}_{\Delta q}$ effects, it does indicate a fundamental problem of the INDI control law applied in this paper. In the derivation of this control law, it is assumed that the influence of the incremental state, Δx, could be neglected. However, as shown in Figure 23, this might not hold for adverse CG locations and therefore could decrease the control performance. Consequently, solving the HQ&S variation of the INDI-based control law for all cases, including adverse CG locations, cannot be fully achieved by finding a correct control effectiveness model alone. Therefore, robust versions of the INDI pitch rate control law, such as Incremental Sliding-mode control [50] or more advanced robust outer loop

Table 7 Incremental pitch acceleration model coefficients, m_α, m_q and m_{δ_e}, for FC-2 and FC-3, and the nominal, forward and aft CG locations.

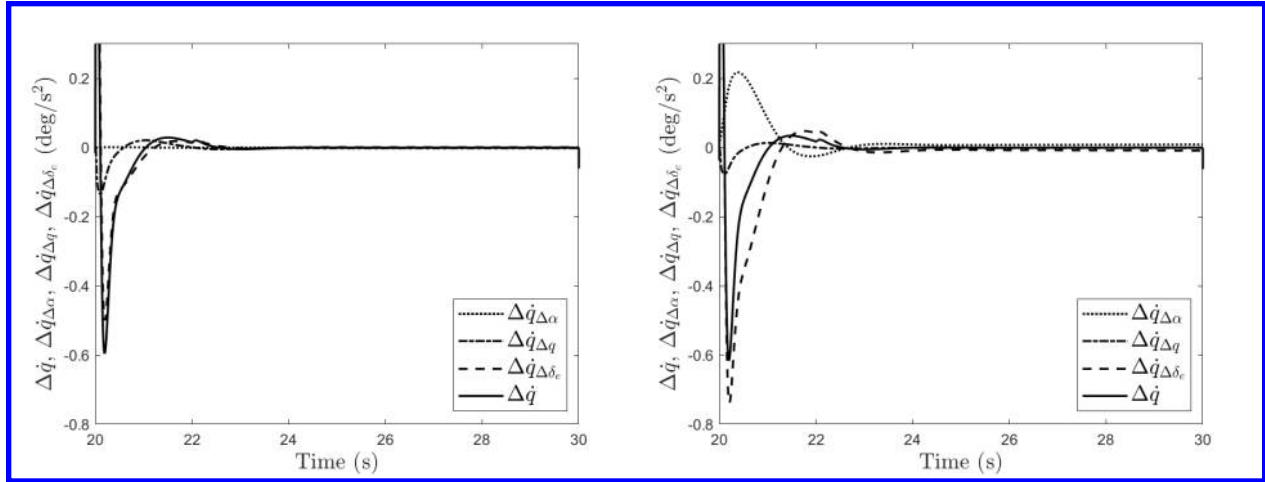|		FC-2			FC-3		
Model coefficient	Unit	nom	fwd	aft	nom	fwd	aft
m_α	s^{-2}	0.0529	-6.43	7.38	0.763	-0.352	3.14
m_q	s^{-2}	-0.949	-1.50	-0.514	-0.471	-0.702	-0.271
m_{δ_e}	s^{-2}	-10.9	-12.5	-11.1	-3.02	-3.40	-3.08

Fig. 22   Incremental pitch acceleration and corresponding incremental state dependency for the nominal CG location of FC-2.

Fig. 23   Incremental pitch acceleration and corresponding incremental state dependency for the aft CG location of FC-2.

designs [51] might aid the required robustness for large CG shifts.

In addition, Wang et al. [21] prove that the influence of the incremental state dependent part becomes less for an increasing sampling frequency, which indicates that an increased sampling frequency could resolve the remaining handling quality variations due to adverse CG shifts. However, this proof is based on the assumption that the actuators and feedback dynamics are ideal. Therefore, the control surface increment determined by the INDI control law could be applied instantly and the feedback signal is neither delayed nor filtered. By contrast, the experiments described here do include actuators and feedback dynamics. In this view, to verify whether an increase in sampling frequency could improve the tracking performance of the control law analysed in this study, the robustness proof developed in Wang et al. [21] should be extended with unmodeled dynamics of actuators and the flight control computer.

Lastly, this study does not consider the effect of noise and turbulence on the parameter estimation performance. As these phenomena distort the signals used by the parameter estimation, it is expected that the estimation performance will degrade and the possible HQ&S variation reduction benefits are weakened. Consequently, it is recommended that effects of these phenomena are investigated in future research to obtain a better understanding of the control performance of the adaptive INDI-based control law considered in this study for real-world applications.

VI. Conclusions and recommendations

This paper presents a handling quality and stability (HQ&S) sensitivity study for an INDI-based pitch rate flight control law. The sensitivity was analyzed for system uncertainties originating from unanticipated centre of gravity (CG) shifts and elevator effectiveness uncertainty. It was confirmed that the control system still shows variations, even though the control law was designed to achieve maximum performance robustness without violating HQ&S guidelines. In an attempt to decrease this variation, an indirect adaptive version of the INDI-based pitch rate control law was proposed and analyzed. The online identification module used in this indirect adaptive control law is based on Least-Mean-Square (LMS) parameter estimation. Furthermore, the objective is to estimate a correction factor to scale the on-board CE model by only using the measured incremental pitch acceleration and incremental elevator deflection feedback. Therefore, the same time-scale separation assumption as used for the INDI control law derivation is applied.

The results obtained for the HQ&S sensitivity analysis of the adaptive control law reveals that online correction of the CE model enables a decrease of the HQ&S variation. However, it is also established that the variation induced by large aft CG shifts cannot be completely solved using this approach. Moreover, for the forward and aft CG location cases at the highest dynamic pressure flight condition, the online parameter estimation performance is degraded as well and shows more activity. The reason behind this problem is an increased influence of the neglected incremental states on the incremental pitch acceleration. Therefore, it is not possible to reach the desired correction factor value by using a model incorporating the time-scale separation assumption. The solution to the estimation problem is to add the incremental state terms to the identification model. However, this result reveals an additional problem considering the

17

INDI pitch rate control law applied in this research. As this control law is also derived using the time-scale separation assumption, the control performance degrades for large CG shifts despite having a correct CE model.

Considering these conclusions there are still some challenges that need to be addressed. First of all, the control performance degradation caused by violation of the time-scale separation assumption due to large CG shifts. The CG location of high-performance aircraft could have a considerable range due to different store configurations. Consequently, this is a very relevant issue for these type of aircraft. Incorporating robust control design frameworks or applying Incremental Sliding-mode control (SMC) [50] might aid in making the control law more robust for large CG shifts. Furthermore, the CE model correction could be improved by incorporating the incremental state influence in the identification model definition. Moreover, coping with turbulence and noise is often a challenging aspect of flight control law design. These stochastic processes can degrade handling qualities and affect parameter estimation performance. Therefore, it is valuable to extend the knowledge obtained in this study by analyzing these phenomena as well. Lastly, a rigorous stability proof of the complete adaptive INDI-based pitch rate control law should be established.

References

[1] Snell, S., Enns, D., and Garrard, W., "Nonlinear inversion flight control for a supermaneuverable aircraft," *Journal of Guidance, Control, and Dynamics*, Vol. 15, No. 4, 1992, pp. 976–984. https://doi.org/10.2514/3.20932.

[2] Gal-Or, B., *Vectored Propulsion, Supermaneuverability and Robot Aircraft*, Springer New York, New York, NY, 1990. https://doi.org/10.1007/978-1-4613-8961-3.

[3] Gallaway, C., and Osborn, R., "Aerodynamics perspective of supermaneuverability," *3rd Applied Aerodynamics Conference*, American Institute of Aeronautics and Astronautics, Colorado Springs,CO,U.S.A., 1985. https://doi.org/10.2514/6.1985-4068.

[4] Slotine, J., and Li, W., *Applied nonlinear control*, Prentice Hall, Englewood Cliffs, N.J, 1991.

[5] Albostan, O., and Gökaşan, M., "High Angle of Attack Manoeuvring Control of F-16 Aircraft Based on Nonlinear Dynamic Inversion and Eigenstructure Assignment," *European Conference for Aeronautics and Space Sciences*, 2017, p. 15. https://doi.org/10.13009/EUCASS2017-228.

[6] Edwards, C., Lombaerts, T., and Smaili, H. (eds.), *Fault tolerant flight control: a benchmark challenge*, 399, Springer, Berlin, 2010.

[7] Mohler, R. R., "Nonlinear Control of High Performance Aircraft," *1993 American Control Conference*, 1993, pp. 1395–1399. https://doi.org/10.23919/ACC.1993.4793100.

[8] Krstić, M., Kanellakopoulos, I., and Kokotović, P. V., *Nonlinear and adaptive control design*, Wiley, 1995.

[9] Miller, C., "Nonlinear Dynamic Inversion Baseline Control Law: Architecture and Performance Predictions," *AIAA Guidance, Navigation, and Control Conference*, American Institute of Aeronautics and Astronautics, Portland, Oregon, 2011. https://doi.org/10.2514/6.2011-6467.

[10] da Costa, R., Chu, Q., and Mulder, J., "Reentry Flight Controller Design Using Nonlinear Dynamic Inversion," *Journal of Spacecraft and Rockets*, Vol. 40, No. 1, 2003, pp. 64–71. https://doi.org/10.2514/2.3916.

[11] Härkegård, O., and Glad, S., "Flight Control Design Using Backstepping," *IFAC Proceedings Volumes*, Vol. 34, No. 6, 2001, pp. 283–288. https://doi.org/10.1016/S1474-6670(17)35187-X.

[12] Steinberg, M., and Page, A., "Nonlinear adaptive flight control with a backstepping design approach," *Guidance, Navigation, and Control Conference and Exhibit*, American Institute of Aeronautics and Astronautics, Boston, MA, USA, 1998. https://doi.org/10.2514/6.1998-4230.

[13] Lombaerts, T., Huisman, H., Chu, Q., Mulder, J., and Joosten, D., "Nonlinear Reconfiguring Flight Control Based on Online Physical Model Identification," *Journal of Guidance, Control, and Dynamics*, Vol. 32, No. 3, 2009, pp. 727–748. https://doi.org/10.2514/1.40788.

[14] van Gils, P., van Kampen, E.-J., de Visser, C. C., and Chu, Q. P., "Adaptive Incremental Backstepping Flight Control for a High-Performance Aircraft with Uncertainties," *AIAA Guidance, Navigation, and Control Conference*, American Institute of Aeronautics and Astronautics, San Diego, CA, USA, 2016. https://doi.org/10.2514/6.2016-1380.

[15] Sieberling, S., Chu, Q. P., and Mulder, J. A., "Robust Flight Control Using Incremental Nonlinear Dynamic Inversion and Angular Acceleration Prediction," *Journal of Guidance, Control, and Dynamics*, Vol. 33, No. 6, 2010, pp. 1732–1742. https://doi.org/10.2514/1.49978.

[16] Smith, P., and Berry, A., "Flight test experience of a non-linear dynamic inversion control law on the VAAC Harrier," *Atmospheric Flight Mechanics Conference*, American Institute of Aeronautics and Astronautics, Denver, CO, USA, 2000. https://doi.org/10.2514/6.2000-3914.

[17] Smeur, E., Chu, Q., and de Croon, G., "Adaptive Incremental Nonlinear Dynamic Inversion for Attitude Control of Micro Air Vehicles," *Journal of Guidance, Control, and Dynamics*, Vol. 39, No. 3, 2016, pp. 450–461. https://doi.org/10.2514/1.G001490.

[18] Grondman, F., Looye, G., Kuchar, R. O., Chu, Q. P., and Van Kampen, E., "Design and Flight Testing of Incremental Nonlinear Dynamic Inversion-based Control Laws for a Passenger Aircraft," *2018 AIAA Guidance, Navigation, and Control Conference*, Kissimmee, FL, USA, 2018. https://doi.org/10.2514/6.2018-0385, AIAA-2018-0385.

[19] Keijzer, T., Looye, G., Chu, Q. P., and Van Kampen, E., "Design and Flight Testing of Incremental Backstepping based Control Laws with Angular Accelerometer Feedback," *AIAA Scitech 2019 Forum*, San Diego, CA, USA, 2019. https://doi.org/10.2514/6.2019-0129, AIAA-2019-0129.

[20] Pollack, T., Looye, G., and van der Linden, F., "Design and flight testing of flight control laws integrating incremental nonlinear dynamic inversion and servo current control," *AIAA Scitech 2019 Forum*, San Diego, CA, USA, 2019. https://doi.org/10.2514/6.2019-0130, AIAA-2019-0130.

[21] Wang, X., van Kampen, E., Chu, Q., and Lu, P., "Stability Analysis for Incremental Nonlinear Dynamic Inversion Control," *Journal of Guidance, Control, and Dynamics*, Vol. 42, No. 5, 2019, pp. 1116–1129. https://doi.org/10.2514/1.G003791.

[22] Gong, A., Tischler, M., and Hess, R., "Deterministic Reconfiguration of Flight Control Systems for Multirotor UAV Package Delivery," *Vertical Flight Society's 77th Annual Forum & Technology Display*, Virtual, 2021.

[23] DoD, *Flying Qualities of Piloted Aircraft*, MIL-HDBK-1797, Department of Defence, 1997.

[24] DoD, "Military Specification: Flying Qualities of Piloted Airplanes, MIL-F-8785C," , November 1980.

[25] Diniz, P. S. R., *Adaptive Filtering: Algorithms and Practical Implementation*, Springer US, 1997.

[26] Haykin, S., and Widrow, B., *Least-Mean-Square Adaptive Filters*, John Wiley & Sons, 2003. Google-Books-ID: U8X3mJtawUkC.

[27] Morelli, E., and Klein, V., *Aircraft System Identification: Theory and Practice*, Sunflyte Enterprises, 2016.

[28] De Visser, C. C., "Global Nonlinear Model Identification with Multivariate Splines," Phd thesis, Delft University of Technology, Faculty of Aerospace Engineering, 2011. ISBN 978-90-8570-770-7.

[29] Tischler, M. B., *Practical Methods for Aircraft and Rotorcraft Flight Control Design: An Optimization-based Approach*, American Institute of Aeronautics and Astronautics, 2017.

[30] AGARD, "Handling Qualities of Unstable Highly Augmented Aircraft," *AGARD-AR-279*, AGARD, Neuilly Sur Seine, France, 1991.

[31] Mitchell, D., Hoh, R., Aponso, B., and Klyde, D., "Proposed Incorporation of Mission-Oriented Flying Qualities into MIL-STD-1797A," Tech. Rep. Wright Laboratory Technical Report (WL-TR-94-3162), 1994.

[32] AGARD, "Flying Qualities," Tech. Rep. AGARD-CP-508, AGARD, feb 1991.

[33] Mitchell, D., Hoh, R., Aponso, B., and Klyde, D., "Flight Control Design - Best Practices," Tech. Rep. Research and Technology Organization Technical Report (RTO-TR-029), 2000.

[34] Berger, T., Tischler, M., Hagerott, S. G., Gangsaas, D., and Saeed, N., "Longitudinal Control Law Design and Handling Qualities Optimization for a Business Jet Flight Control System," *AIAA Atmospheric Flight Mechanics Conference*, American Institute of Aeronautics and Astronautics, 2012. https://doi.org/10.2514/6.2012-4503, URL https://arc.aiaa.org/doi/abs/10.2514/6.2012-4503.

[35] Neal, T. P., and Smith, R. E., "An In-flight Investigation to Develop Control System Design Criteria for Fighter Airplanes," Tech. Rep. AFFDL-TR-70-74, Volume 2, Air Force Flight Dynamics Laboratory, Dec. 1970.

[36] Skogestad, S., and Postlethwaite, I., *Multivariable Feedback Control: Analysis and Design*, Wiley, 2005.

[37] Stevens, B., Lewis, F., and Johnson, E., *Aircraft Control and Simulation: Dynamics, Controls Design, and Autonomous Systems*, Wiley, 2015.

[38] Sun, L. G., "Model and Sensor Based Nonlinear Adaptive Flight Control with Online System Identification," Ph.D. thesis, Delft University of Technology, Faculty of Aerospace Engineering, 2014. ISBN 978-94-6186-350-8.

[39] Heise, C. D., Leitao, M., and Holzapfel, F., "Performance and Robustness Metrics for Adaptive Flight Control - Available Approaches," *AIAA Guidance, Navigation, and Control (GNC) Conference*, American Institute of Aeronautics and Astronautics, Boston, MA, USA, 2013. https://doi.org/10.2514/6.2013-5090.

[40] Bhardwaj, P., Akkinapalli, V. S., Zhang, J., Saboo, S., and Holzapfel, F., "Adaptive Augmentation of Incremental Nonlinear Dynamic Inversion Controller for an Extended F-16 Model," *AIAA Scitech 2019 Forum*, American Institute of Aeronautics and Astronautics, San Diego, CA, USA, 2019. https://doi.org/10.2514/6.2019-1923.

[41] Stepanyan, V., Krishnakumar, K., Nguyen, N., and van Eykeren, L., "Stability and Performance Metrics for Adaptive Flight Control," *AIAA Guidance, Navigation, and Control Conference*, American Institute of Aeronautics and Astronautics, Chicago, IL, USA, 2009. https://doi.org/10.2514/6.2009-5965.

[42] Mooij, E., "Robust Control of a Conventional Aeroelastic Launch Vehicle," *AIAA Scitech 2020 Forum*, American Institute of Aeronautics and Astronautics, Orlando, FL, 2020. https://doi.org/10.2514/6.2020-1103.

[43] Muir, E., "The GARTEUR High Incidence Research Model (HIRM) benchmark problem," *Guidance, Navigation, and Control Conference and Exhibit*, American Institute of Aeronautics and Astronautics, Boston, MA, USA, 1998. https://doi.org/10.2514/6.1998-4243.

[44] DoD, *Flight Control Systems - Design, Installation and Test of Piloted Aircraft*, MIL-DTL-9490E, Department of Defence, 2008.

[45] Nguyen, L., Ogburn, M., Gilbert, W., Kibler, K., Brown, P., and Deal, P., "Simulator Study of Stall/Post-Stall Characteristics of a Fighter Airplane With Relaxed Longitudinal Static Stability," Tech. rep., National Aeronautics and Space Administration, Langley Research Center, Hampton, Virginia, 1979.

[46] Russel, R., "Non-linear F-16 Simulation using Simulink and Matlab," Tech. rep., University of Minnesota, June 2003.

[47] van 't Veld, R., van Kampen, E., and Chu, Q., "Stability and Robustness Analysis and Improvements for Incremental Nonlinear Dynamic Inversion Control," *2018 AIAA Guidance, Navigation, and Control Conference*, American Institute of Aeronautics and Astronautics, Kissimmee, FL, USA, 2018. https://doi.org/10.2514/6.2018-1127.

[48] Leith, D., and Leithead, W., "Survey of gain-scheduling analysis and design," *International Journal of Control*, Vol. 73, 2000, pp. 1001–1025. https://doi.org/10.1080/002071700411304.

[49] Sonneveldt, L., "Adaptive Backstepping Flight Control for Modern Fighter Aircraft," Ph.D. thesis, Delft University of Technology, Faculty of Aerospace Engineering, 2010. ISBN 978-90-8570-573-4.

[50] Wang, X., van Kampen, E., and Chu, Q. P., "Incremental Sliding-Mode Fault-Tolerant Flight Control," *Journal of Guidance, Control, and Dynamics*, Vol. 42, No. 2, 2019. https://doi.org/10.2514/1.G003497.

[51] Magni, J., Bennani, S., and Terlouw, J., *Robust Flight Control - A Design Challenge*, Lecture Notes in Control and Information Sciences (LNCIS), Vol. 224, Springer, 1997.